


Article

A Novel Three-Phase Power Flow Algorithm for the Evaluation of the Impact of Renewable Energy Sources and D-STATCOM Devices on Unbalanced Radial Distribution Networks

Raavi Satish ¹, Kanchapogu Vaisakh ², Almoataz Y. Abdelaziz ³ and Adel El-Shahat ^{4,*} 

¹ Department of Electrical and Electronics Engineering, Anil Neerukonda Institute of Technology and Science, Visakhapatnam 531162, Andhra Pradesh, India; satish.eee@anits.edu

² Department of Electrical Engineering, Andhra University, Visakhapatnam 530003, Andhra Pradesh, India; prof.kvaisakh@andhrauniversity.edu.in

³ Faculty of Engineering and Technology, Future University in Egypt, Cairo 11835, Egypt; almoataz.abdelaziz@fue.edu.eg

⁴ Energy Technology Program, School of Engineering Technology, Purdue University, West Lafayette, IN 47907, USA

* Correspondence: asayedah@purdue.edu



Citation: Satish, R.; Vaisakh, K.; Abdelaziz, A.Y.; El-Shahat, A. A Novel Three-Phase Power Flow Algorithm for the Evaluation of the Impact of Renewable Energy Sources and D-STATCOM Devices on Unbalanced Radial Distribution Networks. *Energies* **2021**, *14*, 6152. <https://doi.org/10.3390/en14196152>

Academic Editor: Zhiwei Liu

Received: 31 August 2021

Accepted: 23 September 2021

Published: 27 September 2021

Publisher's Note: MDPI stays neutral with regard to jurisdictional claims in published maps and institutional affiliations.



Copyright: © 2021 by the authors. Licensee MDPI, Basel, Switzerland. This article is an open access article distributed under the terms and conditions of the Creative Commons Attribution (CC BY) license (<https://creativecommons.org/licenses/by/4.0/>).

Abstract: The impacts of the fast growth of renewable energy sources (RESs) and distribution static synchronous compensators (D-STATCOMs) on unbalanced radial distribution networks (URDNs) are analyzed with three-phase power flow algorithms (PFAs). As the URDNs are unbalanced, they can experience voltage unbalance (VU). This paper proposes a novel three-phase PFA for URDNs with multiple RES and D-STATCOM device integrations. The bus number matrix (BNM) and branch number matrix (BRNM) developed in this paper make the implementation of the proposed PFA simple. These matrices are developed to store the bus numbers and branch numbers of newly created sections of the URDN. Both PQ and PV modeling of RES and PV modeling of D-STATCOM devices are effectively integrated into the proposed three-phase PFA. The accuracy of the proposed PFA has been tested on the IEEE-13 bus URDN and the results are found to be accurate with the IEEE results. Several study examples have been conducted on the IEEE-13 bus and the IEEE-34 bus URDNs with multiple integrations of three-phase RESs and three-phase D-STATCOMs. Test results indicate that these integrations improve the voltage profile, reduce the power loss and reduce the severity of the VU.

Keywords: unbalanced distribution networks; renewable energy sources; distribution static synchronous compensator; voltage unbalance; power flow algorithm

1. Introduction

RESs, such as solar, wind, fuel cells, etc., use synchronous generators (SGs)/induction generators (IGs), IGs combined with power electronic converters (PECs) or only PECs to transfer AC power to the grids. The unbalanced nature in distribution networks is because of the asymmetrical conductor spacing and the uneven distribution of single-phase and two-phase loads on the network. Hence, they can have VU problems. The severity of VU problems with a high penetration of single-phase photovoltaic systems into secondary radial distribution networks is presented in [1]. In [2], a mitigation strategy to restrict the VU based on distributed batteries included in grid-interfaced PV rooftop systems is presented. The authors of [3] propose a new power angle control (PAC) algorithm designed to simplify the control algorithm and obtain a fast, dynamic response. It also expands the PAC's capacity to compensate for VU with or without phase-angle jump in a simple way. Using this PAC strategy, the power quality issues such as sag, swell and imbalances of source voltage, load reactive power and harmonics in distribution networks are enhanced by a unified power quality conditioner (UPQC). The authors of [4] used the

three-phase AC optimal power flow (OPF) formulation to reduce the VU using reactive power from solar PV inverters. It analyzes the impact of different VU measures using different combinations of VU objectives and constraints. The authors of [5] propose a three-phase power flow method for a real-time distribution system. It gives the initial discussions on a PV node concept in a three-phase power flow based on a compensation method. In [6], a novel current-injection-based Newton–Raphson PFA for improving the convergence characteristics is presented with a new PV bus. The connection of distributed generation (DG) with the utility grid is specified in the IEEE-1547 standard [7]. The authors of [8–11] present the optimal placement and sizing of DGs for URDNs. In [12], different optimization algorithms are used to demonstrate the impact of optimum allocations of renewable DGs on distribution networks. The authors of [13] analyzed the centralized control techniques to decrease the impact of DG and electric vehicles and improve their efficient integration. In [14], the voltage profile, QV sensitivity analysis and QV curve analysis for a grid with high RES penetration are presented.

The power quality of the network is improved by compensating the reactive power through shunt-connected distribution flexible AC transmission systems (DFACTSs), such as D-STATCOMs. Some work has been done in modeling the D-STATCOM for power flow analysis [15–17]. The authors of [18] present a probabilistic technique for optimal allocation of the D-STATCOM in distribution networks containing correlated RESs. In [19] an optimal step, a least mean squares algorithm for controlling three-phase D-STATCOMs, is presented. It provides harmonic compensation in addition to reactive power compensation in three-phase linear and non-linear loads. The authors of [20] present a literature survey on the optimal allocation of D-STATCOMs in distribution networks. The authors of [21] present the main effects of the DG connection to a grid and the role of STATCOMs to minimize the undesirable effects, making the DG fully operable. In [22], the influence of FACTS device implementation on the performance of distribution networks with RES integration is presented. The authors of [23] present a three-phase PFA for URDN with combined integration of DGs and D-STATCOM devices by developing BUS_NUM and BRANCH_NUM matrices.

This paper develops a BNM and BRNM to store the information of bus numbers and branch numbers, respectively, of newly divided sections of the URDN. The URDN is divided into new sections by exploiting its radial topology. The proposed, novel three-phase PFA with multiple RESs and D-STATCOM device integrations make use of these matrices. The remaining paper is arranged as follows. Modeling for the network components is addressed in Section 2. The VU is discussed in Section 3. The algorithm for developing the BNM and BRNM is presented in Section 4. The three-phase PFA with the multiple RESs and D-STATCOM devices is discussed in Section 5. The test results and discussions for various case studies on IEEE-13 and IEEE-34 bus URDNs are addressed in Section 6. The concluding remarks are discussed in Section 7.

2. Materials and Modeling of Network Components

This section provides a brief modeling of distribution network components such as power lines, transformers, loads, capacitor banks, RESs and D-STATCOMs.

2.1. Modeling of Lines

The Carson equations and Kron reduction [24] will develop the phase matrices of size 3×3 for overhead and underground lines with grounded neutrals. The phase matrices for 2-phase and 1-phase lines will have zero entries instead of missing phases.

Figure 1 represents the exact three-phase model of power lines. In Equation (1), the phase voltage matrix at bus 'k' is expressed with the phase voltage matrix at bus 'j' and the phase impedance matrix as well as the phase current matrix for the branch 'jk'.

$$\begin{bmatrix} V_a \\ V_b \\ V_c \end{bmatrix}_k = \begin{bmatrix} V_a \\ V_b \\ V_c \end{bmatrix}_j - \begin{bmatrix} Z_{aa} & Z_{ab} & Z_{ac} \\ Z_{ba} & Z_{bb} & Z_{bc} \\ Z_{ca} & Z_{cb} & Z_{cc} \end{bmatrix}_{jk} \bullet \begin{bmatrix} I_a \\ I_b \\ I_c \end{bmatrix}_{jk} \quad (1)$$

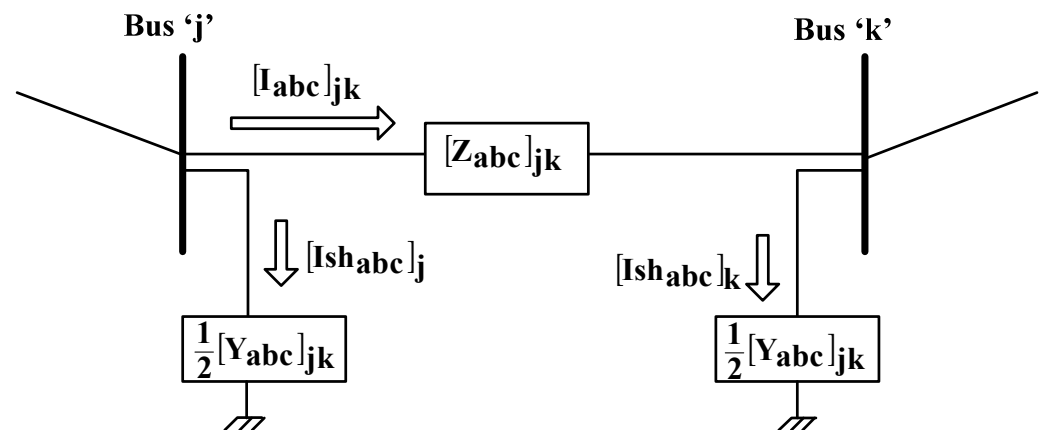


Figure 1. Exact model of three-phase line.

Equation (2) gives the phase current matrix for serving the shunt admittance at bus 'k'.

$$\begin{bmatrix} I_{sh_a} \\ I_{sh_b} \\ I_{sh_c} \end{bmatrix}_k = \frac{1}{2} \begin{bmatrix} Y_{aa} & Y_{ab} & Y_{ac} \\ Y_{ba} & Y_{bb} & Y_{bc} \\ Y_{ca} & Y_{cb} & Y_{cc} \end{bmatrix}_{jk} \bullet \begin{bmatrix} V_a \\ V_b \\ V_c \end{bmatrix}_k \quad (2)$$

2.2. Modeling of Loads

The detailed modeling for the calculation of line current matrix for three-phase spot loads and modeling of distributed loads is presented in [23,24].

2.3. Modeling of Capacitor Banks

In [24,25], the details of Table 1 are presented. The line current matrix serving the three-phase capacitor banks are presented in Table 2.

Table 1. Modeling of capacitor banks.

	Wye Connected	Delta Connected
Specified phase voltage matrix at a bus and reactive power matrix	$\begin{bmatrix} V_{an} \angle \delta_a \\ V_{bn} \angle \delta_b \\ V_{cn} \angle \delta_c \end{bmatrix}, \begin{bmatrix} Q_a \\ Q_b \\ Q_c \end{bmatrix}$	$\begin{bmatrix} V_{ab} \angle \delta_{ab} \\ V_{bc} \angle \delta_{bc} \\ V_{ca} \angle \delta_{ca} \end{bmatrix}, \begin{bmatrix} Q_{ab} \\ Q_{bc} \\ Q_{ca} \end{bmatrix}$
Phase current matrix serving the capacitor bank	$[B_{abc}] = \begin{bmatrix} \frac{Q_a}{ V_{an} ^2} \\ \frac{Q_b}{ V_{bn} ^2} \\ \frac{Q_c}{ V_{cn} ^2} \end{bmatrix}$ $\begin{bmatrix} I_{C_a} \\ I_{C_b} \\ I_{C_c} \end{bmatrix} = \begin{bmatrix} j \bullet B_a \bullet V_{an} \\ j \bullet B_b \bullet V_{bn} \\ j \bullet B_c \bullet V_{cn} \end{bmatrix}$	$[B_{abc}] = \begin{bmatrix} \frac{Q_{ab}}{ V_{ab} ^2} \\ \frac{Q_{bc}}{ V_{bc} ^2} \\ \frac{Q_{ca}}{ V_{ca} ^2} \end{bmatrix}$ $\begin{bmatrix} I_{C_{ab}} \\ I_{C_{bc}} \\ I_{C_{ca}} \end{bmatrix} = \begin{bmatrix} j \bullet B_{ab} \bullet V_{ab} \\ j \bullet B_{bc} \bullet V_{bc} \\ j \bullet B_{ca} \bullet V_{ca} \end{bmatrix}$

Table 1. Cont.

	Wye Connected	Delta Connected
Line current matrix serving the capacitor bank	$\begin{bmatrix} IC_a \\ IC_b \\ IC_c \end{bmatrix}$	$\begin{bmatrix} IC_a \\ IC_b \\ IC_c \end{bmatrix} = \begin{bmatrix} 1 & 0 & -1 \\ -1 & 1 & 0 \\ 0 & -1 & 1 \end{bmatrix} \bullet \begin{bmatrix} IC_{ab} \\ IC_{bc} \\ IC_{ca} \end{bmatrix}$

Table 2. RES models for PFAs.

RES Type	Electric Machine	Utility Interface	Suitable Model for PFAs	Explanations
Fuel cell		Inverter	PV bus	CCC is intended to independently control P and V
			PQ bus	CCC is intended to independently control P and Q
Solar		Inverter	PV bus	CCC is intended to independently control P and V
			PQ bus	CCC is intended to independently control P and Q
Wind	FSIG	Directly	PQ bus	-
			SVCM	
	DFIG	Rectifier + Inverter	PV bus	CCC is intended to independently control P and V
			PQ bus	CCC is intended to independently control P and Q
	Conventional or permanent magnet SG	Rectifier + Inverter	PV bus	CCC is intended to independently control P and V
			PQ bus	CCC is intended to independently control P and Q
Hydro	SG	Directly	PV bus	VEV in FTV
			PQ bus	VEV in FPF
			SVCM	CEV
Geothermal	SG	Directly	PV bus	VEV in FTV
			PQ bus	VEV in FPF
			SVCM	CEV
Biofuel	SG	Directly	PV bus	VEV in FTV
			PQ bus	VEV in FPF
			SVCM	CEV

2.4. Modeling of Three-Phase Transformers

The authors of [26] present the matrix relationships among primary and secondary sides with various connections on primary and secondary sides of three-phase transformers.

2.5. Renewable Energy Source

The type of equipment used to connect the RES to the network relies on its application and the type of power source used. Normally, a modest diesel generator requires a SG, and a wind turbine may require a fixed-speed induction generator (FSIG) or a double-fed induction generator (DFIG) or a PEC-connected generator. PV systems and fuel cells use a PEC to connect them to the network. The RES modeling for PFAs requires the knowledge of operation and interfacing equipment characteristics. Interfacing equipment's

brief modeling is presented in the subsequent sections. Table 2 summarizes the different RES types and their interconnection methods to the grids as well as their models tailored to PFAs.

2.5.1. Synchronous Generator

SGs are of two types according to the excitation system [27,28]. The former is the constant excitation voltage (CEV) type and the latter is the variable excitation voltage (VEV) type. The excitation voltage is controlled by two methods for the VEV type. The first method is to keep the fixed terminal voltage (FTV) mode and the second method is to keep the fixed power factor (FPF) mode. In PFAs, the SG with first method is treated as a PV bus and the SG with the second method is treated as a PQ bus.

Take the example of a round-rotor SG to model the CEV SGs. The reactive power (Q) of DG is presented in Equation (3):

$$Q = \sqrt{\left(\frac{E_q}{X_d}\right)^2 - P^2} - \frac{V^2}{X_d} \quad (3)$$

Taking the active power (P) of DG as constant,

$$P = P_s = \text{constant}$$

$$Q = f(V)$$

The SGs without the VEV type may inject Q into the network when Q is positive in the above expression. Therefore, the SVCMM may be used to model this SG.

2.5.2. Induction Generator

Both P and Q in IGs are functions of voltage and slip [29].

$$P = f(V, s)$$

$$Q = f(V, s)$$

Taking P as constant and neglecting the very small reliance of Q on the slip, the expression above may be reduced as below,

$$P = P_s = \text{constant}$$

$$Q = f(V).$$

The SVCMM suits the above equations for PFAs. For steady-state cases the IG can be modeled as a PQ bus, because the voltages at buses are near 1 p.u.

2.5.3. Power Electronic Converter

The PEC modeling for PFAs depends on the control method used in the converter control circuit (CCC). If the CCC is intended to independently control P and V , then model the PEC as a PV bus [28]. If the CCC is intended to independently control P and Q , then model the PEC as a PQ bus [30].

2.6. D-STATCOM

The enhancement in current and voltage management abilities of power electronic equipment have permitted the development of FACTS devices. Therefore, the prospects have emerged in utilizing various kinds of controllers for effective shunt and series compensation. The FACTS concept was initially developed for transmission systems, but a similar concept has begun to be applied to distribution networks. The D-STATCOM device is coupled in shunts with the network and it compensates power quality problems in short time periods. In this period, the D-STATCOM can supply both P and Q to the network. The

D-STATCOM must be provided with an energy storage system to supply P to the network. For the steady-state application, the power exchange between D-STATCOMs and the AC system is Q .

The D-STATCOM is commonly regarded as a shunt compensator which supplies Q in PFAs. The voltage magnitude at a D-STATCOM bus can be controlled by adjusting the Q injection of D-STATCOMs.

The interface of a D-STATCOM at the i -th bus shown in Figure 2a and its traditional modeling for PFAs is shown in Figure 2b. The specified Q of load is combined with the Q output of the D-STATCOM, so that Q varies as the magnitude of V_i varies. This is absolutely a PV bus model, with the P output of the D-STATCOM set to zero [16,17]. The hypothesis in this model is that losses in the D-STATCOM and its connection are ignored.

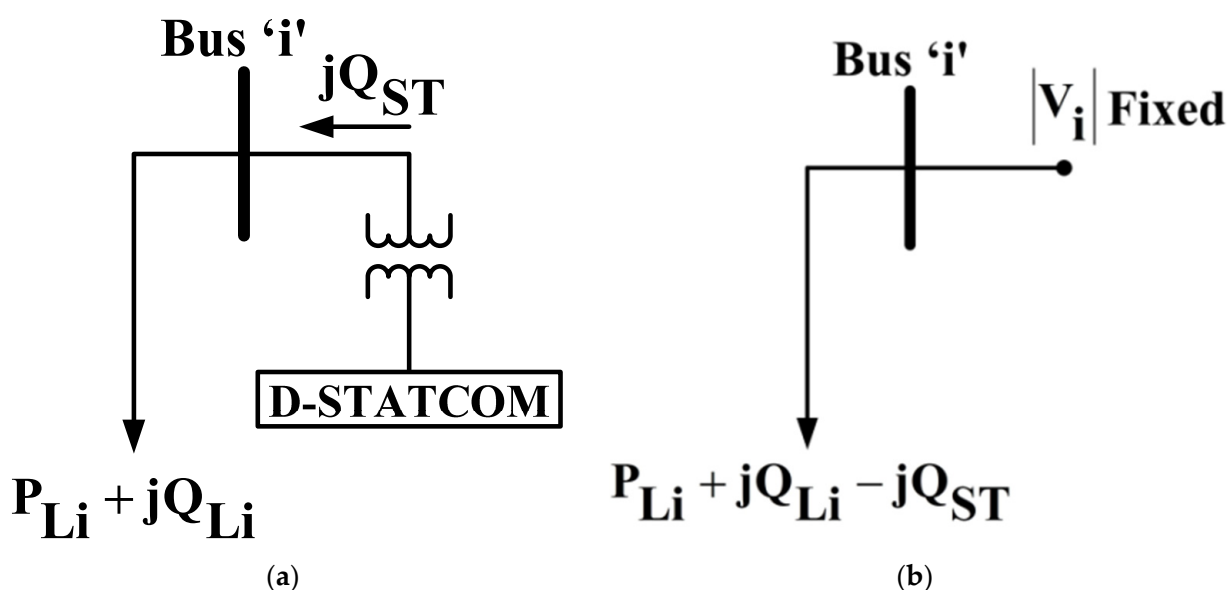


Figure 2. (a) D-STATCOM interface at i -th bus. (b) Traditional modeling of a D-STATCOM as a PV bus.

3. Voltage Unbalance

VU is a usual problem in URDNs. An increase in VU can create overheating and de-rating of induction motor loads as well as create network problems, such as mal-operation of protective relays and harmonics generation from power electronic loads [31]. Several methods have been used to define and elucidate the voltage unbalance factor (VUF) [32]. The actual definition of VUF is given in Equation (4). International standards of allowable VU limits are presented in [1].

$$VUF\% = \left(\frac{V_2}{V_1} \right) \cdot 100 \quad (4)$$

where,

V_2 : Negative sequence component of voltage;

V_1 : Positive sequence component of voltage.

4. Algorithm for Developing the BNM and BRNM

The performance of the PFA of URDNs is enhanced by systematic numbering of buses and branches. From [33], the numbering scheme for buses and branches is taken. The following steps are to be followed in order to write a software code to split URDNs into different sections, as shown in Figure 3.

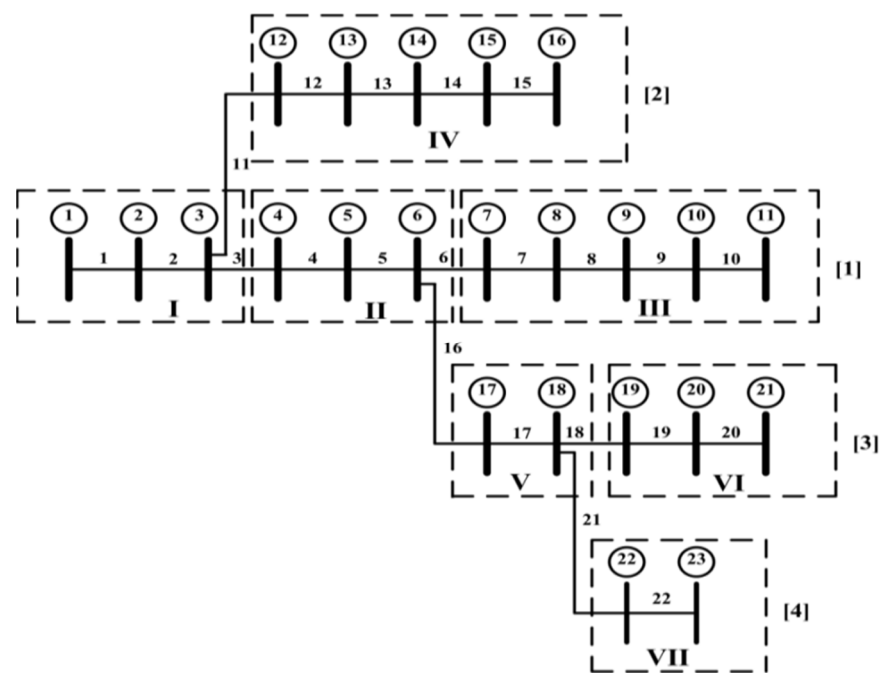


Figure 3. Divided sections for sample distribution network.

1. Using the distribution network shown in Figure 3, construct Table 3.

Table 3. Branch numbering of the distribution network in Figure 3.

Branch Number (BN)	Sending Bus (SE)	Receiving Bus (RE)
1	1	2
2	2	3
3	3	4
4	4	5
5	5	6
6	6	7
7	7	8
8	8	9
9	9	10
10	10	11
11	3	12
12	12	13
13	13	14
14	14	15
15	15	16
16	6	17
17	17	18
18	18	19
19	19	20
20	20	21
21	18	22
22	22	23

2. Starting with $BN = 1$, read the RE of the BN, i.e., 2. Then, check how many times this 2 appears in the SE row. From the above table it appeared once. That means bus 2 is the sending end for only one branch. Fill these RE 2 and BN 1 into two different variables (BNM and BRNM) as the first row and first column elements. Then, increase the column number by one.
3. Increase the BN (i.e., $BN = 2$), read the RE of the BN, i.e., 3. Then, as in step 1, check for the appearance of 3 in the SE row. Bus 3 appeared twice. That means that two branches leave from bus 3. Then, fill these RE 3 and BN 2 into the same variables as the first row and present the column elements. Name this row's elements as section-I. Now increase the row number by one and set the column number to one.
4. Similarly, increase the BN, read the RE of the BN. Then, check for the appearance of this RE in the SE row. If it appears once, then fill these RE and BN values in as the present row and present column elements of variables BNM and BRNM. Then, increase the column number by one. Repeat step 4. If it does not appear or does appear more than one time in the SE row, then fill the corresponding RE and BN values as present row and present column elements. Then, identify this row as a section. Then, increase the row number by one and set the column number to one. Additionally, repeat step 4.

The above steps are repeated until the BN value reaches the last branch number. At the end, the variables BNM and BRNM are obtained as follows.

$$\begin{aligned}
 \text{BNM} &= \begin{bmatrix} 1 & 2 & 3 & 0 & 0 \\ 4 & 5 & 6 & 0 & 0 \\ 7 & 8 & 9 & 10 & 11 \\ 12 & 13 & 14 & 15 & 16 \\ 17 & 18 & 0 & 0 & 0 \\ 19 & 20 & 21 & 0 & 0 \\ 22 & 23 & 0 & 0 & 0 \end{bmatrix} \begin{matrix} \rightarrow \text{Section-I} \\ \rightarrow \text{Section-II} \\ \rightarrow \text{Section-III} \\ \rightarrow \text{Section-IV} \\ \rightarrow \text{Section-V} \\ \rightarrow \text{Section-VI} \\ \rightarrow \text{Section-VII} \end{matrix} \\
 \text{BRNM} &= \begin{bmatrix} 1 & 2 & 0 & 0 & 0 \\ 3 & 4 & 5 & 0 & 0 \\ 6 & 7 & 8 & 9 & 10 \\ 11 & 12 & 13 & 14 & 15 \\ 16 & 17 & 0 & 0 & 0 \\ 18 & 19 & 20 & 0 & 0 \\ 21 & 22 & 0 & 0 & 0 \end{bmatrix} \begin{matrix} \rightarrow \text{Section-I} \\ \rightarrow \text{Section-II} \\ \rightarrow \text{Section-III} \\ \rightarrow \text{Section-IV} \\ \rightarrow \text{Section-V} \\ \rightarrow \text{Section-VI} \\ \rightarrow \text{Section-VII} \end{matrix}
 \end{aligned}$$

5. Three-Phase PFA with RESs and D-STATCOMs

After the development of the BNM and BRNM for the URDN, the iterative scheme for the PFA is explained by the following steps:

1. Set iteration number $\gamma = 1$.
2. Set iteration number $r = 1$.
3. All bus voltages are allocated as the voltage at the sub-station bus.

$$\begin{bmatrix} V_a \\ V_b \\ V_c \end{bmatrix} = \begin{bmatrix} 1\angle 0^\circ \\ 1\angle -120^\circ \\ 1\angle 120^\circ \end{bmatrix} p.u \quad (5)$$

4. Find the line current matrix serving the load at all buses.
5. Start with the collecting line current matrix at bus-23 (the tail bus in section-VII in the BNM) thereby find the line current matrix for branch-22 (the tail branch in section-VII in the BRNM). Then, continue to bus-22 and branch-21 to find the line current matrix at the bus and the line current matrix in the branch, respectively. From Figure 4, the following equations are obtained by applying KCL at every bus:

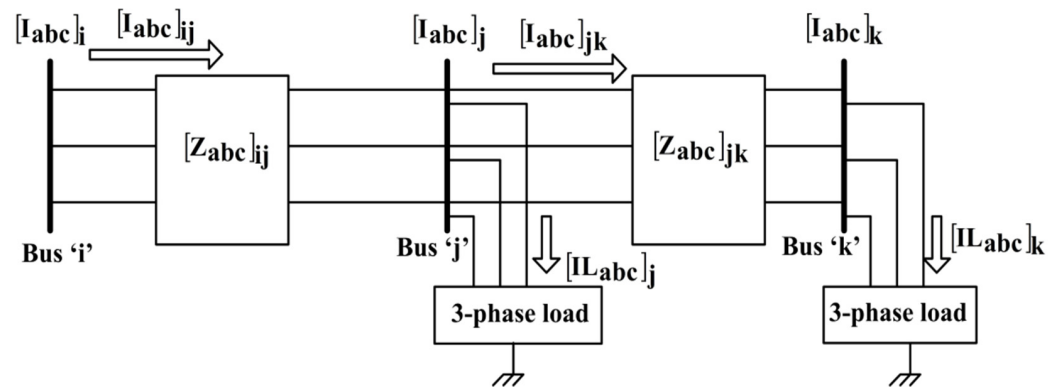


Figure 4. A simple URDN with three busses.

$$[I_{abc}]_k = [IL_{abc}]_k + [Ish_{abc}]_k + [IC_{abc}]_k - [I_{RES,abc}]_j^\gamma \quad (6)$$

$$[I_{abc}]_{jk} = [I_{abc}]_k \quad (7)$$

$$[I_{abc}]_j = [I_{abc}]_{jk} + [IL_{abc}]_j + [Ish_{abc}]_j + [IC_{abc}]_j \quad (8)$$

$$[I_{abc}]_{ij} = [I_{abc}]_j \quad (9)$$

$$[I_{abc}]_i = [I_{abc}]_{ij} \quad (10)$$

where,

$[I_{abc}]_k$: line current matrix at bus-k;

$[I_{abc}]_{jk}$: line current matrix for branch-jk;

$[IL_{abc}]_k$: line current matrix for load at bus-k;

$[Ish_{abc}]_k$: line current matrix for shunt admittance at bus-k;

$[IC_{abc}]_k$: line current matrix for capacitor bank at bus-k, if any;

$[I_{RES,abc}]_j^\gamma$: line current matrix injected by an RES or a D-STATCOM at busk, if any (for $\gamma = 1$, take this current injection as zero).

6. Now go to section-VI and repeat the procedure as in step 5 to find the line current matrix at the head bus and the line current matrix for the head branch. Similarly, proceed to upto section-I and find the line current matrix upto bus-1 and the line current matrix upto branch-1.
7. Now start with the head bus in section-I and continue to the tail bus in section-1 by finding the phase voltage matrix at all buses with Equation (1). Then, go to the next section and repeat the same procedure.
8. Steps 4 to 7 are to be repeated until the convergence criterion as given in Equation (11) is satisfied:

$$\left| [V_{abc}]_i^r - [V_{abc}]_i^{r-1} \right| \leq [\epsilon_{abc}] \quad (11)$$

9. Locations of both the RES and D-STATCOM are to be selected.

10. Examine the RES type for the γ -th outside iteration.
11. If at the j -th bus the modeling of the RES is PQ, then the line current injection matrix at that bus is calculated with Equation (12):

$$[I_{\text{RES},abc}]_j^\gamma = \begin{bmatrix} (S_{\text{RES},a}/V_a)^* \\ (S_{\text{RES},b}/V_b)^* \\ (S_{\text{RES},c}/V_c)^* \end{bmatrix}_j^\gamma \quad (12)$$

12. If the modeling of the RES and D-STATCOM device at a bus is PV, then mismatches in voltages are calculated with Equation (13):

$$\begin{bmatrix} \Delta V_a \\ \Delta V_b \\ \Delta V_c \end{bmatrix}^\gamma = \begin{bmatrix} V_a^{\text{sp}} \\ V_b^{\text{sp}} \\ V_c^{\text{sp}} \end{bmatrix} - \begin{bmatrix} V_a^{\text{cal}} \\ V_b^{\text{cal}} \\ V_c^{\text{cal}} \end{bmatrix} \quad \forall \text{PV buses} \quad (13)$$

$$[\Delta V_{abc}]^\gamma \leq [\varepsilon_{abc}] \quad (14)$$

where $[\Delta V_{abc}]^\gamma$ is the matrix of phase voltage mismatches with size $3 \cdot n \times 1$.

13. If Equation (14) is not satisfied at PV buses, then in order to maintain the specified voltages at these buses, the incremental current injection matrices are obtained with Equation (15):

$$[\Delta I]^\gamma = [Z_{\text{PV}}]^{-1} \cdot [\Delta V]^\gamma \quad (15)$$

where $[Z_{\text{PV}}]$ is the sensitivity matrix for a PV bus with a size of $3 \cdot n \times 3 \cdot n$. The formation of this matrix is presented in [5].

14. If the RES and D-STATCOM device are able to generate unlimited Q, then the incremental reactive current injection matrix at the j -th PV bus is calculated with Equation (16):

$$\begin{bmatrix} \Delta I_{\text{RES},a} \\ \Delta I_{\text{RES},b} \\ \Delta I_{\text{RES},c} \end{bmatrix}_j^\gamma = \begin{bmatrix} |\Delta I_a| \cdot (\cos(90^\circ + \delta_{v,a}) + j \cdot \sin(90^\circ + \delta_{v,a})) \\ |\Delta I_b| \cdot (\cos(90^\circ + \delta_{v,b}) + j \cdot \sin(90^\circ + \delta_{v,b})) \\ |\Delta I_c| \cdot (\cos(90^\circ + \delta_{v,c}) + j \cdot \sin(90^\circ + \delta_{v,c})) \end{bmatrix}_j^\gamma \quad (16)$$

15. As displayed in Figure 5, by applying KCL at the j -th bus, the line current matrix for branch 'ij' can be obtained with Equation (17):

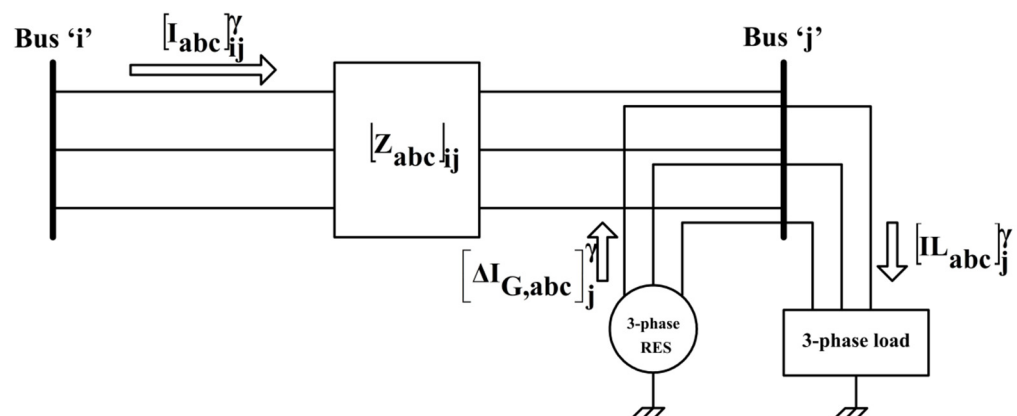


Figure 5. A simple URDN with two buses with the RES placed at the j -th bus.

$$\begin{bmatrix} I_a \\ I_b \\ I_c \end{bmatrix}_{ij}^\gamma = \begin{bmatrix} I_{La} \\ I_{Lb} \\ I_{Lc} \end{bmatrix}_j^\gamma - \begin{bmatrix} \Delta I_{G,a} \\ \Delta I_{G,b} \\ \Delta I_{G,c} \end{bmatrix}_j^\gamma \quad (17)$$

With $[V_{abc}]_j^\gamma$ and $[I_{abc}]_{ij}^\gamma$, the matrix for Q flow in the 'ij' branch is evaluated. Now, the incremental reactive power injection matrix is obtained with Equation (18):

$$\begin{bmatrix} \Delta Q_{RES,a} \\ \Delta Q_{RES,b} \\ \Delta Q_{RES,c} \end{bmatrix}_j = \begin{bmatrix} QL_a \\ QL_b \\ QL_c \end{bmatrix}_j - \begin{bmatrix} Q_a \\ Q_b \\ Q_c \end{bmatrix}_{ij} \quad (18)$$

The Q generation matrix required at the j-th PV bus is calculated by using Equation (19):

$$\begin{bmatrix} Q_{RES,a} \\ Q_{RES,b} \\ Q_{RES,c} \end{bmatrix}_j = \begin{bmatrix} Q_{RES,a} \\ Q_{RES,b} \\ Q_{RES,c} \end{bmatrix}_j^{\gamma-1} + \begin{bmatrix} \Delta Q_{RES,a} \\ \Delta Q_{RES,b} \\ \Delta Q_{RES,c} \end{bmatrix}_j \quad (19)$$

With Equation (20), at the PV bus the matrix for complex power generation can be calculated:

$$\begin{bmatrix} S_{RES,a} \\ S_{RES,b} \\ S_{RES,c} \end{bmatrix}_j = \begin{bmatrix} P_{RES,a} \\ P_{RES,b} \\ P_{RES,c} \end{bmatrix}_j + j \cdot \begin{bmatrix} Q_{RES,a} \\ Q_{RES,b} \\ Q_{RES,c} \end{bmatrix}_j \quad (20)$$

The specified P generation $[P_{RES,abc}]_j$ for the D-STATCOM device is set to zero.

16. The injected line current matrix at the RES and D-STATCOM device is obtained with Equation (12) by using the matrix for complex power generation given in Equation (20).
17. If the RES and D-STATCOM device are able to generate limited Q, then find the total Q generation of the RES and D-STATCOM device with Equation (21). The total Q generation of the RES and D-STATCOM device is now compared with the maximum and minimum limits of Q generation of the RES and D-STATCOM device, respectively. Limits:

$$(Q_{RES})_j^\gamma = (Q_{RES,a})_j^\gamma + (Q_{RES,b})_j^\gamma + (Q_{RES,c})_j^\gamma$$

If $Q_{j,\min} \leq (Q_{RES})_j^\gamma \leq Q_{j,\max}$

(21)

Then, set the complex power generation as in Equation (20)

$$\text{If } (Q_{RES})_j^\gamma \leq Q_{j,\min} \quad (22)$$

Then, set $(Q_{RES})_j^\gamma = Q_{j,\min}$ and $(Q_{RES,a})_j^\gamma = (Q_{RES,b})_j^\gamma = (Q_{RES,c})_j^\gamma = Q_{j,\min}/3$

If $(Q_{RES})_j^\gamma \geq Q_{j,\max}$

Then, set $(Q_{RES})_j^\gamma = Q_{j,\max}$ and $(Q_{RES,a})_j^\gamma = (Q_{RES,b})_j^\gamma = (Q_{RES,c})_j^\gamma = Q_{j,\max}/3$

Combine these Q generations with the P generations of the RES and D-STATCOM device and find the line current injection matrix at PV buses using Equation (12).

18. Using the line current injection matrix at all PV buses, repeat from step 3 by setting $\gamma = \gamma + 1$.
19. Stop the iterative procedure when the convergence criteria is attained for every PV bus as given by Equation (14).
20. The complex power loss matrix for each branch is calculated with Equation (23).

$$\begin{bmatrix} S_{Loss_a} \\ S_{Loss_b} \\ S_{Loss_c} \end{bmatrix}_{ij} = \begin{bmatrix} (V_a)_i \cdot (I_a)_{ij}^* \\ (V_b)_i \cdot (I_b)_{ij}^* \\ (V_c)_i \cdot (I_c)_{ij}^* \end{bmatrix} - \begin{bmatrix} (V_a)_j \cdot (I_a)_{ji}^* \\ (V_b)_j \cdot (I_b)_{ji}^* \\ (V_c)_j \cdot (I_c)_{ji}^* \end{bmatrix} \quad (23)$$

21. Find the total power loss of the network and VUF% at each bus by using Equation (4).

Figure 6 presents the flowchart for this algorithm.

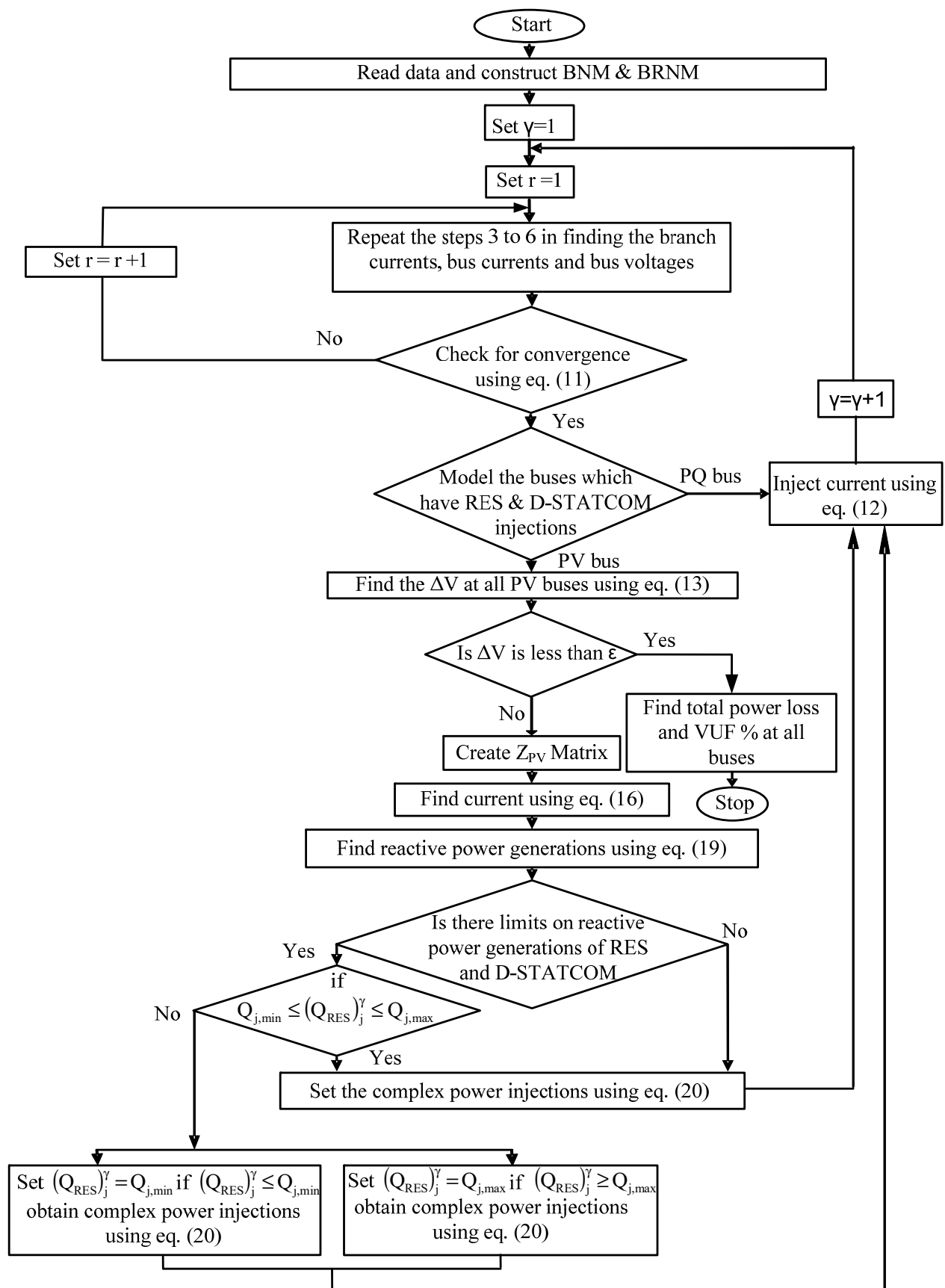


Figure 6. Flowchart for the proposed three-phase PFA.

6. Results and Discussions

6.1. IEEE-13 Bus URDN

The proposed three-phase PFA is examined on an IEEE-13 bus unbalanced test feeder without interfacing of the RES and D-STATCOM device. Figure 7 shows the IEEE-13 bus feeder, and its data is collected from [34]. The chosen base values for this network are 5000 kVA and 4.16 kV. The PFA convergence takes five iterations, with a tolerance for convergence of 10^{-4} . Table 4 presents the comparison of obtained power loss with the IEEE losses. The comparison of the obtained power flow solution with the IEEE solution and errors in voltage magnitudes and phase angles at every bus are presented in Table 5. Insignificant values of maximum errors of 0.0005 p.u and 0.010° for voltage magnitudes and phase angles are observed in Table 5. In terms of accuracy, the test results are consistent with IEEE results.

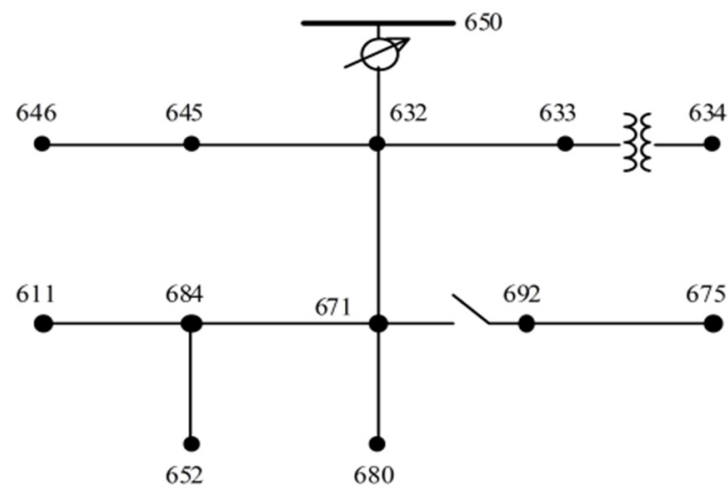


Figure 7. IEEE-13 bus URDN.

Table 4. Power loss comparison for the IEEE-13 bus URDN.

Phase	Obtained Power Loss		IEEE Losses [34]	
	P Loss (kW)	Q Loss (kVAR)	P Loss (kW)	Q Loss (kVAR)
a	39.13	152.62	39.18	152.59
b	−4.74	42.27	−4.70	42.22
c	76.59	129.69	76.65	129.85
Total	110.98	324.57	111.13	324.66

Table 5. Comparison of power flow solution with the IEEE solution for the IEEE-13 bus URDN.

Bus	Phase	Obtained Voltage Solution	IEEE Solution [34]	Error in Voltage Mag.	Error in Voltage Ang.
650	a	$1<0^\circ$	$1<0^\circ$	0.0000	0.00
	b	$1<-120^\circ$	$1<-120^\circ$	0.0000	0.00
	c	$1<120^\circ$	$1<120^\circ$	0.0000	0.00
RG	a	$1.0625<0^\circ$	$1.0625<0^\circ$	0.0000	0.00
	b	$1.0500<-120^\circ$	$1.0500<-120^\circ$	0.0000	0.00
	c	$1.0687<120^\circ$	$1.0687<120^\circ$	0.0000	0.00
632	a	$1.0210<-2.49^\circ$	$1.0210<-2.49^\circ$	0.0000	0.00
	b	$1.0420<-121.72^\circ$	$1.0420<-121.72^\circ$	0.0000	0.00
	c	$1.0175<117.83^\circ$	$1.0170<117.83^\circ$	−0.0005	0.00

Table 5. Cont.

Bus	Phase	Obtained Voltage Solution	IEEE Solution [34]	Error in Voltage Mag.	Error in Voltage Ang.
671	a	0.9900<−5.30°	0.9900<−5.30°	0.0000	0.00
	b	1.0529<−122.34°	1.0529<−122.34°	0.0000	0.00
	c	0.9778<116.03°	0.977<116.02°	0.0001	−0.01
680	a	0.9900<−5.30°	0.9900<−5.30°	0.0000	0.00
	b	1.0529<−122.34°	1.0529<−122.34°	0.0000	0.00
	c	0.9778<116.03°	0.977<116.02°	0.0001	−0.01
633	a	1.0180<−2.55°	1.0180<−2.56°	0.0000	0.01
	b	1.0401<−121.77°	1.0401<−121.77°	0.0000	0.00
	c	1.0148<117.82°	1.0148<117.82°	0.0000	0.00
634	a	0.9940<−3.23°	0.9940<−3.23°	0.0000	0.00
	b	1.0218<−122.22°	1.0218<−122.22°	0.0000	0.00
	c	0.9960<117.35°	0.9960<117.34°	0.0000	−0.01
645	b	1.0328<−121.90°	1.0329<−121.90°	0.0001	0.00
	c	1.0155<117.86°	1.0155<117.86°	0.0001	0.00
646	b	1.0311<−121.98°	1.0311<−121.98°	0.0000	0.00
	c	1.0134<117.90°	1.0134<117.90°	0.0000	0.01
692	a	0.9900<−5.30°	0.9900<−5.31°	0.0000	0.01
	b	1.0529<−122.34°	1.0529<−122.34°	0.0000	0.00
	c	0.9778<116.03°	0.9777<116.02°	−0.0001	−0.01
675	a	0.9835<−5.55°	0.9835<−5.56°	0.0000	0.01
	b	1.0553<−122.52°	1.0553<−122.52°	0.0000	0.00
	c	0.9759<116.04°	0.9758<116.03°	−0.0001	−0.01
684	a	0.9881<−5.32°	0.9881<−5.32°	0.0000	0.00
	c	0.9758<115.92°	0.9758<115.92°	0.0000	0.00
611	c	0.9738<115.78°	0.9738<115.78°	0.0000	0.00
652	a	0.9825<−5.24°	0.9825<−5.25°	0.0000	0.01

6.2. IEEE-13 Bus URDN with Study Examples

The specification of the RES and D-STATCOM device for different study examples are presented in Table 6. The rating and location of the RES and D-STATCOM presented in Table 6 are taken from [23]. The obtained total P loss and total Q loss on the network for different study examples are presented in Table 7. It is observed in study example one, that is, without the integration of the RES and D-STATCOM device, the P loss and Q loss are found to be 147.33 kW and 433.54 kVAR, and these losses are reduced to 64.90 kW and 174.27 kVAR with the integration of two RESs and one D-STATCOM device for study example one. Table 8 presents the obtained voltage solution and VUF% for the study examples one, two and three. It is observed that voltage profile improvement is more in study example3.

Table 6. Study examples of the IEEE-13 bus URDN.

Study Examples		Specification		
Example1		<ul style="list-style-type: none"> • Voltage regulator is taken off between bus-650 and bus-632 • Capacitor banks are taken off at bus-675 and bus-611 		
	Device	Location	Modeling	Rating [23]
Example2	Three-phase RES	Bus-634	PQ	P = 300 kW/phase and Q = 197 kVAR/phase
	Three-phase RES	Bus-675	PV	P = 260 kW/phase and 3-phase Q limits: $100 \leq Q \leq 650$ kVAR
Example3	Three-phase RES	Bus-634	PQ	P = 300 kW/phase and Q = 197 kVAR/phase
	Three-phase RES	Bus-675	PV	P = 260 kW/phase and 3-phase Q limits: $100 \leq Q \leq 650$ kVAR
	Three-phase D-STATCOM	Bus-680	PV	P = 0 and 3-phase Q limits: $100 \leq Q \leq 500$ kVAR

Table 7. Power loss comparison for different study examples of the IEEE-13 bus URDN.

Phase	Example-1		Example-2		Example-3	
	P Loss (kW)	Q Loss (kVAR)	P Loss (kW)	Q Loss (kVAR)	P Loss (kW)	Q Loss (kVAR)
A	39.48	194.82	7.9867	87.6800	7.9589	83.4026
B	−2.03	47.13	4.0219	10.1590	2.9510	9.6542
C	109.88	191.59	56.8390	88.4051	53.9973	81.2180
Total	147.33	433.54	68.84	186.24	64.90	174.27

Table 8. Obtained voltage solution and VUF% for different study examples of the IEEE-13 bus URDN.

Bus	S. No	Ph	Example1		Example2		Example3	
			$ V_{p.u} /\angle \text{deg}$	VUF%	$ V_{p.u} /\angle \text{deg}$	VUF%	$ V_{p.u} /\angle \text{deg}$	VUF%
650	1	a	$1 < 0^\circ$		$1.0000 < 0^\circ$		$1.0000 < 0^\circ$	
	2	b	$1 < -120^\circ$	0	$1.0000 < -120^\circ$	0	$1.0000 < -120^\circ$	0
	3	c	$1 < 120^\circ$		$1.0000 < 120^\circ$		$1.0000 < 120^\circ$	
632	4	a	$0.9498 < -2.74^\circ$		$0.9730 < -1.68^\circ$		$0.9752 < -1.73^\circ$	
	5	b	$0.9839 < -121.68^\circ$	1.27	$0.9973 < -120.48^\circ$	0.83	$0.9994 < -120.49^\circ$	0.81
	6	c	$0.9300 < 117.80^\circ$		$0.9540 < 118.98^\circ$		$0.9566 < 118.92^\circ$	
671	7	a	$0.9109 < -5.89^\circ$		$0.9429 < -4.10^\circ$		$0.9474 < -4.19^\circ$	
	8	b	$0.9875 < -122.20^\circ$	2.58	$1.0045 < -120.42^\circ$	1.89	$1.0088 < -120.44^\circ$	1.88
	9	c	$0.8717 < 115.95^\circ$		$0.9056 < 117.88^\circ$		$0.9109 < 117.77^\circ$	
680	10	a	$0.9109 < -5.89^\circ$		$0.9429 < -4.10^\circ$		$0.9485 < -4.22^\circ$	
	11	b	$0.9875 < -122.20^\circ$	2.58	$1.0045 < -120.42^\circ$	1.89	$1.0099 < -120.45^\circ$	1.88
	12	c	$0.8717 < 115.95^\circ$		$0.9056 < 117.87^\circ$		$0.9121 < 117.74^\circ$	
633	13	a	$0.9466 < -2.82^\circ$		$0.9749 < -1.64^\circ$		$0.9772 < -1.69^\circ$	
	14	b	$0.9819 < -121.73^\circ$	1.28	$1.0006 < -120.40^\circ$	0.82	$1.0027 < -120.42^\circ$	0.81
	15	c	$0.9271 < 117.79^\circ$		$0.9574 < 119.06^\circ$		$0.9600 < 119.01^\circ$	
634	16	a	$0.9207 < -3.60^\circ$		$0.9950 < -1.00^\circ$		$0.9972 < -1.05^\circ$	
	17	b	$0.9624 < -122.24^\circ$	1.35	$1.0249 < -119.60^\circ$	0.76	$1.0270 < -119.62^\circ$	0.76
	18	c	$0.9064 < 117.21^\circ$		$0.9828 < 119.94^\circ$		$0.9853 < 119.88^\circ$	
645	19	b	$0.9745 < -121.86^\circ$		$0.9880 < -120.66^\circ$		$0.9901 < -120.67^\circ$	
	20	c	$0.9283 < 117.82^\circ$		$0.9523 < 119.00^\circ$		$0.9549 < 118.95^\circ$	

Table 8. Cont.

Bus	S. No	Ph	Example1		Example2		Example3	
			$ V_{p.u} /\angle \text{deg}$	VUF%	$ V_{p.u} /\angle \text{deg}$	VUF%	$ V_{p.u} /\angle \text{deg}$	VUF%
646	21	b	0.9729<−121.93°		0.9863<−120.73°		0.9884<−120.75°	
	22	c	0.9264<117.86°		0.9503<119.05°		0.9529<118.99°	
692	23	a	0.9109<−5.89°		0.9429<−4.10°		0.9474<−4.19°	
	24	b	0.9875<−122.20°	2.58	1.0045<−120.42°	1.89	1.0088<−120.44°	1.88
	25	c	0.8717<115.95°		0.9056<117.87°		0.9109<117.77°	
675	26	a	0.9025<−6.07°		0.9379<−4.19°		0.9424<−4.28°	
	27	b	0.9887<−122.30°	2.75	1.0080<−120.44°	2.00	1.0123<−120.47°	1.99
	28	c	0.8678<116.06°		0.9047<118.08°		0.9099<117.97°	
684	29	a	0.9093<−5.95°		0.9411<−4.15°		0.9456<−4.24°	
	30	c	0.8684<115.91°		0.9023<117.84°		0.9076<117.74°	
611	31	c	0.8651<115.83°		0.8990<117.77°		0.9043<117.66°	
652	32	a	0.9041<−5.87°		0.9358<−4.07°		0.9403<−4.17°	

6.3. Discussion

It is noted for study example one from Table 9 that the maximum VUF% is 2.75 at bus-675 and the minimum value of voltage is 0.8651 p.u at bus-611 for the cphase. The results of this study are not desirable. In study example two, an improvement in the minimum value of voltage at bus-611 for the cphase is observed with its value of 0.8990 p.u., and there is a reduction in maximum VUF% to 2 at bus-675. In study example three, an improvement in the minimum value of voltage at bus-611 for the cphase is observed with its value of 0.9043 p.u., and there is a reduction in the maximum VUF% to 1.99 at bus-675. Figure 8 shows the voltage profile comparison for different study examples with serial numbers on the network. The voltage profile is poor for study example one, that is, without the RES and D-STATCOM device integration, and the voltage profile is improved in study example two and study example three.

Table 9. Study examples of the IEEE-34 bus URDN.

Study Examples	Specification			
Example1	<ul style="list-style-type: none"> • Voltage regulator is taken off between bus-614 and bus-650 and bus-852–bus-832. • Capacitor banks are taken off at bus-844 and bus-848. 			
	Device	Location	Modeling	Rating
Example2	Three-phase RES	Bus-848	PQ	P = 150 kW/phase and Q = 99 kVAR/phase
	Three-phase D-STATCOM	Bus-650	PV	P = 0 and 3-phase Q limits: $50 \leq Q \leq 250$ kVAR.
Example3	Three-phase RES	Bus-848	PQ	P = 150 kW/phase and Q = 99 kVAR/phase
	Three-phase RES	Bus-890	PV	P = 130 kW/phase and 3-phase Q limits: $50 \leq Q \leq 325$ kVAR.
	Three-phase D-STATCOM	Bus-650	PV	P = 0 and 3-phase Q limits: $50 \leq Q \leq 250$ kVAR.

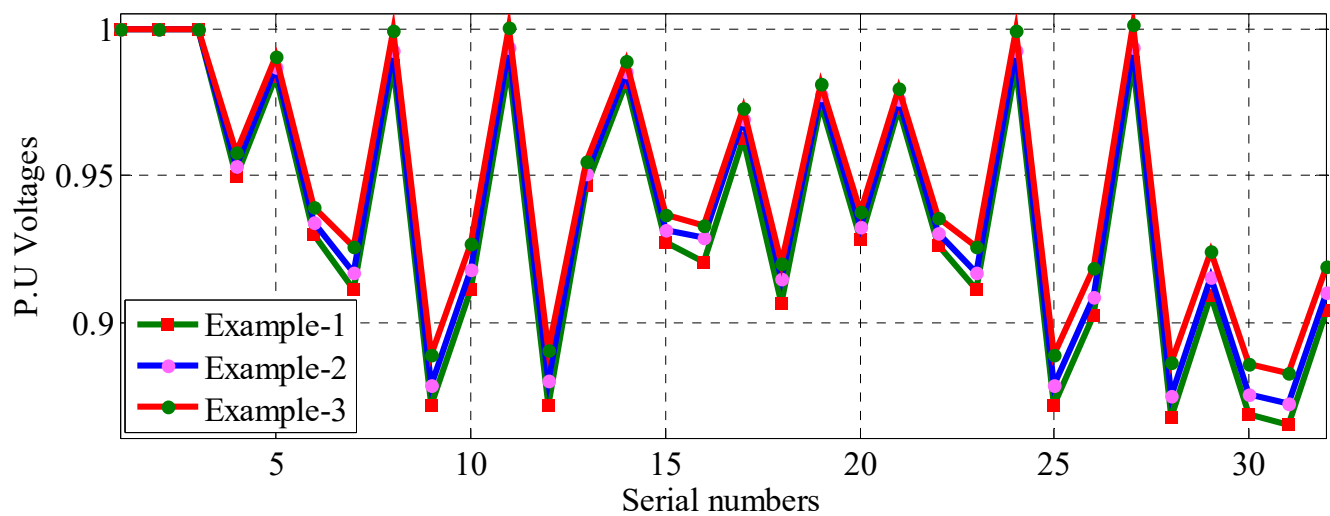


Figure 8. Comparison of voltage profiles for different study examples of the IEEE-13 bus URDN.

6.4. Study Examples and Discussion of the IEEE-34 Bus URDN

Figure 9 shows the IEEE-34 bus URDN, and its data is presented in [34]. The chosen base values for this network are 2500 kVA and 4.9 kV. The PFA convergence takes two iterations, with a tolerance for convergence of 10^{-4} . The specification of the RES and D-STATCOM device for different study examples are presented in Table 9. Figure 10 shows the voltage profile comparison for different study examples with serial numbers on the network. It is observed from Figure 10 that the voltage profile of the network is poor in study example one, that is, without the RES and D-STATCOM device integration. For study example two, where two RESs are integrated, the voltage profile is improved. For study example three, with two RESs and one D-STATCOM device integration, the voltage profile is further improved. Figure 11 compares the minimum value of voltage on the network in different study examples. The minimum voltage on the network is 0.7837 p.u for study example one, and the minimum voltage on the network is improved to 0.8386 p.u and 0.903 p.u for study example two and study example three, respectively. Figure 12 compares the power loss in different study examples. The P loss and Q loss of the network are 260.89 kW and 180.49 kVAR, respectively, for study example one. For study example two, the P loss and Q loss are reduced to 123.46 kW and 94.23 kVAR, respectively. For study example three, these losses are further reduced to 56.48 kW and 37.73 kVAR. Figure 13 compares the maximum VUF% in different study examples. It is observed that the maximum VUF% on the network is 1.3 for study example one. For study example two, the maximum VUF% is reduced to 1.12, and for study example three the maximum VUF% is further reduced to 0.98. Therefore, from the results of these study examples on the IEEE-34 bus URDN it is observed that network has low power loss, a high minimum value of voltage on the network and a low value of maximum VUF% for study example three, in which two RESs and one D-STATCOM device are integrated into the network.

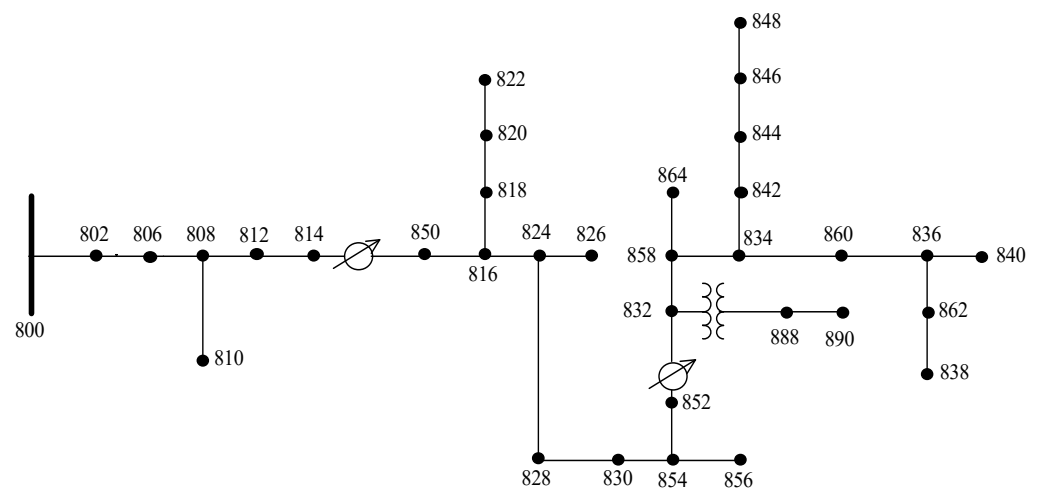


Figure 9. IEEE-34 bus URDN.

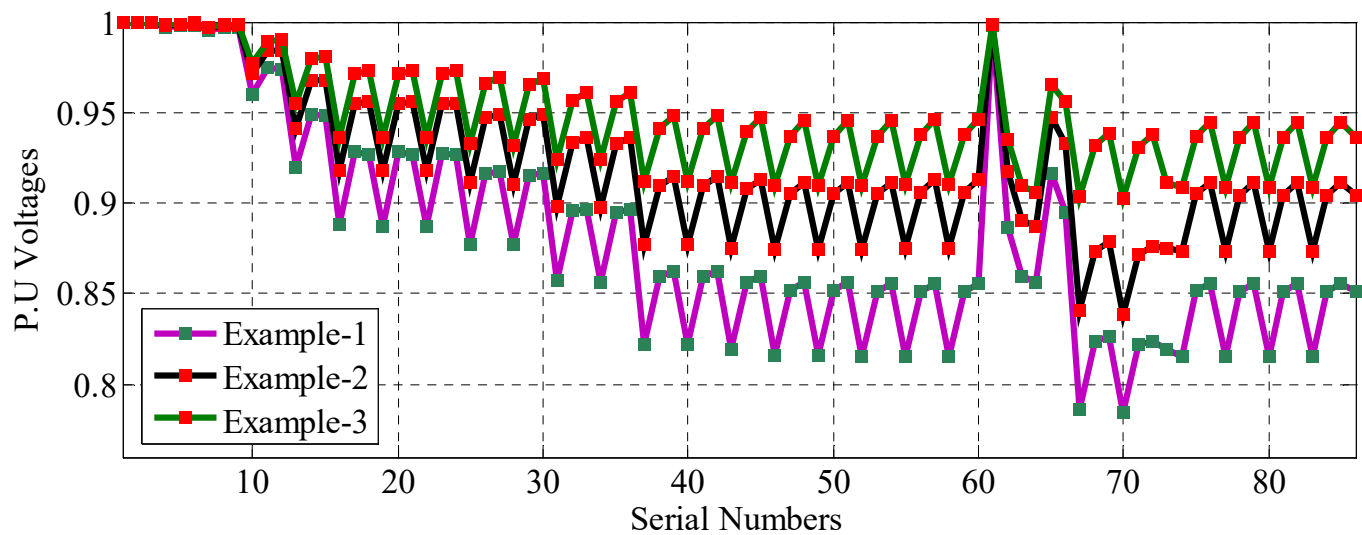


Figure 10. Voltage profile comparison in different study examples of the IEEE-34 bus URDN.

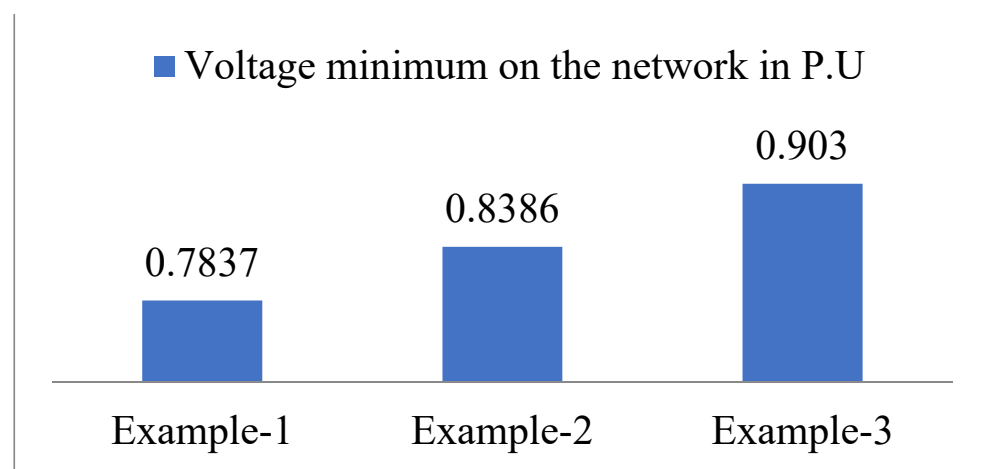


Figure 11. Voltage minimum in different study examples of the IEEE-34 bus URDN.

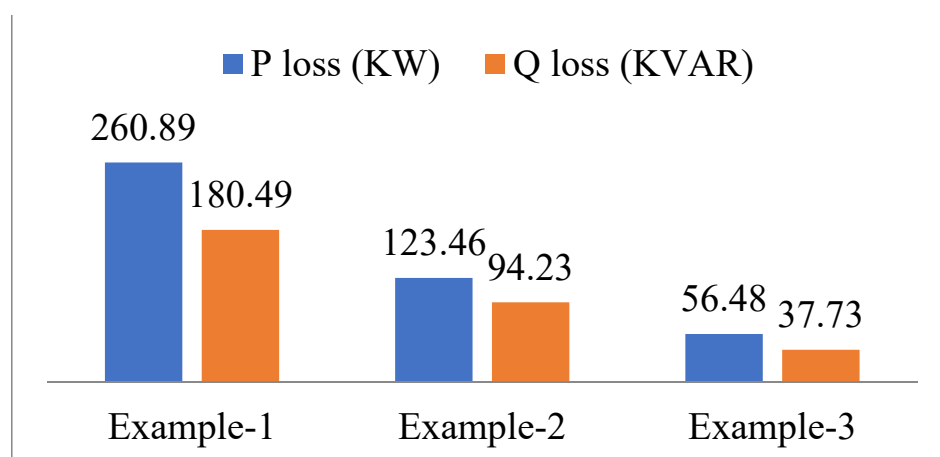


Figure 12. Power loss comparison in different study examples of the IEEE-34 bus URDN.

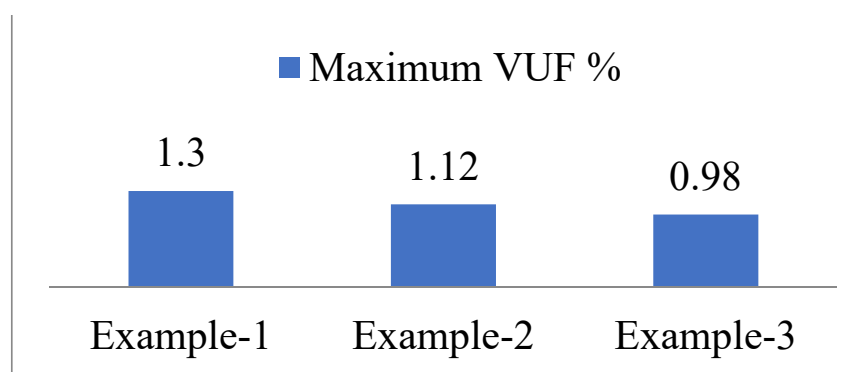


Figure 13. Maximum VUF% in different study examples of the IEEE-34 bus URDN.

7. Conclusions

The execution of the proposed three-phase PFA becomes simple by using the BNM and BRNM for its implementation. The PFA's accuracy is tested on an IEEE-13 bus unbalanced test feeder without RES and D-STATCOM device interfacing. It is found that insignificant values of maximum errors of 0.0005 p.u and 0.010° for voltage magnitudes and phase angles are observed, therefore the proposed PFA is accurate with the IEEE results. The PV and PQ modeling of RES and PV modeling of D-STATCOM devices are efficiently handled by the proposed PFA. Different study examples are conducted on IEEE-13 bus and IEEE-34 bus URDNs. Results of the study examples show that voltage profile improvement, power loss reduction and decrease in severity of VUF% are obtained with the integration of the RES and D-STATCOM device. Finding the inverse of a sensitivity matrix will become complex as the number of PV buses in the network increases. Because the sensitivity matrix consists of complex numbers as its entries, there is therefore a limitation with two PV buses in this paper. Furthermore, the work can be extended to find the optimal sizing and placement of RES and D-STATCOM devices by applying any optimization algorithm to this three-phase PFA.

Author Contributions: R.S. and K.V. designed the problem under study, performed the simulations and obtained the results. R.S. and K.V. wrote the paper, which was further reviewed by A.Y.A. and A.E.-S. All authors have read and agreed to the published version of the manuscript.

Funding: This research received no external funding.

Conflicts of Interest: The authors declare no conflict of interest.

References

- Rodríguez, F.J.R.; Hernandez, J.C.; Jurado, F. Voltage unbalance assessment in secondary radial distribution networks with single-phase photovoltaic systems. *Int. J. Electr. Power Energy Syst.* **2015**, *64*, 646–654. [\[CrossRef\]](#)
- Nour, A.M.; Helal, A.A.; El-Saadawi, M.M.; Hatata, A.Y. A control scheme for voltage unbalance mitigation in distribution network with rooftop PV systems based on distributed batteries. *Int. J. Electr. Power Energy Syst.* **2021**, *124*, 106375. [\[CrossRef\]](#)
- Abdoli, O.; Gholipour, E.; Hooshmand, R.-A. A New Approach to Compensating Voltage Unbalance by UPQC-Based PAC. *Electr. Power Compon. Syst.* **2018**, *46*, 1769–1781. [\[CrossRef\]](#)
- Girigoudar, K.; Roald, L.A. On the impact of different voltage unbalance metrics in distribution system optimization. *Electr. Power Syst. Res.* **2020**, *189*, 106656. [\[CrossRef\]](#)
- Cheng, C.S.; Shirmohammadi, D. A three-phase power flow method for real-time distribution system analysis. *IEEE Trans. Power Syst.* **1995**, *10*, 671–679. [\[CrossRef\]](#)
- Kumar, A.; Jha, B.K.; Singh, D.; Misra, R.K. A New Current Injection Based Power Flow Formulation. *Electr. Power Compon. Syst.* **2020**, *48*, 268–280. [\[CrossRef\]](#)
- IEEE. *IEEE Standard for Interconnecting Distributed Resources with Electric Power Systems*; IEEE: Piscataway, NJ, USA, 2003; pp. 1–28. [\[CrossRef\]](#)
- Abdelaziz, A.Y.; Hegazy, Y.G.; El-Khattam, W.; Othman, M.M. A Multi-objective Optimization for Sizing and Placement of Voltage-controlled Distributed Generation Using Supervised Big Bang–Big Crunch Method. *Electr. Power Compon. Syst.* **2015**, *43*, 105–117. [\[CrossRef\]](#)
- Othman, M.M.; Hegazy, Y.; Abdelaziz, A. Electrical energy management in unbalanced distribution networks using virtual power plant concept. *Electr. Power Syst. Res.* **2017**, *145*, 157–165. [\[CrossRef\]](#)
- Abdelaziz, A.Y.; Hegazy, Y.G.; El-Khattam, W.; Othman, M.M. Optimal Planning of Distributed Generators in Distribution Networks Using Modified Firefly Method. *Electr. Power Compon. Syst.* **2015**, *43*, 320–333. [\[CrossRef\]](#)
- Abdelaziz, A.; Hegazy, Y.; El-Khattam, W.; Othman, M. Optimal allocation of stochastically dependent renewable energy based distributed generators in unbalanced distribution networks. *Electr. Power Syst. Res.* **2015**, *119*, 34–44. [\[CrossRef\]](#)
- Tolba, M.A.; Rezk, H.; Tulskey, V.; Diab, A.A.Z.; Abdelaziz, A.Y.; Vanin, A. Impact of Optimum Allocation of Renewable Distributed Generations on Distribution Networks Based on Different Optimization Algorithms. *Energies* **2018**, *11*, 245. [\[CrossRef\]](#)
- Serem, N.; Letting, L.; Munda, J. Voltage Profile and Sensitivity Analysis for a Grid Connected Solar, Wind and Small Hydro Hybrid System. *Energies* **2021**, *14*, 3555. [\[CrossRef\]](#)
- Zarco-Soto, F.; Zarco-Periñán, P.; Martínez-Ramos, J. Centralized Control of Distribution Networks with High Penetration of Renewable Energies. *Energies* **2021**, *14*, 4283. [\[CrossRef\]](#)
- Gotham, D.J.; Heydt, G.T. Power flow control and power flow studies for systems with FACTS devices. *IEEE Trans. Power Syst.* **1998**, *13*, 60–65. [\[CrossRef\]](#)
- Yang, Z.; Shen, C.; Crow, M.L.; Zhang, L. An improved STATCOM model for power flow analysis. In Proceedings of the Power Engineering Society Summer Meeting, Seattle, WA, USA, 16–20 July 2000; Volume 2, pp. 1121–1126. [\[CrossRef\]](#)
- Jazebi, S.; Hosseini, S.; Vahidi, B. DSTATCOM allocation in distribution networks considering reconfiguration using differential evolution algorithm. *Energy Convers. Manag.* **2011**, *52*, 2777–2783. [\[CrossRef\]](#)
- Rezaeian-Marjani, S.; Galvani, S.; Talavat, V.; Farhadi-Kangarlu, M. Optimal allocation of D-STATCOM in distribution networks including correlated renewable energy sources. *Int. J. Electr. Power Energy Syst.* **2020**, *122*, 106178. [\[CrossRef\]](#)
- Patel, S.K.; Arya, S.R.; Maurya, R. Optimal Step LMS-Based Control Algorithm for DSTATCOM in Distribution System. *Electr. Power Compon. Syst.* **2019**, *47*, 675–691. [\[CrossRef\]](#)
- Sirjani, R.; Jordehi, A.R. Optimal placement and sizing of distribution static compensator (D-STATCOM) in electric distribution networks: A review. *Renew. Sustain. Energy Rev.* **2017**, *77*, 688–694. [\[CrossRef\]](#)
- Sayahi, K.; Kadri, A.; Bacha, F.; Marzougui, H. Implementation of a D-STATCOM control strategy based on direct power control method for grid connected wind turbine. *Int. J. Electr. Power Energy Syst.* **2020**, *121*, 106105. [\[CrossRef\]](#)
- Relić, F.; Marić, P.; Glavaš, H.; Petrović, I. Influence of FACTS Device Implementation on Performance of Distribution Network with Integrated Renewable Energy Sources. *Energies* **2020**, *13*, 5516. [\[CrossRef\]](#)
- Satish, R.; Kantarao, P.; Vaisakh, K. A new algorithm for impacts of multiple DGs and D-STATCOM in unbalanced radial distribution networks. *Int. J. Renew. Energy Technol.* **2021**, *12*, 221. [\[CrossRef\]](#)
- Kersting, W.H. *Distribution System Modeling and Analysis*, 4th ed.; CRC Press: Boca Raton, FL, USA, 2017.
- Khushalani, S. Unbalanced distribution power flow with distributed generation. In Proceedings of the IEEE/PES Transactions on Distribution Conference, Dallas, TX, USA, 21–24 May 2006; pp. 301–306. [\[CrossRef\]](#)
- Chen, T.-H.; Chen, M.-S.; Inoue, T.; Kotas, P.; Chebli, E. Three-phase cogenerator and transformer models for distribution system analysis. *IEEE Trans. Power Deliv.* **1991**, *6*, 1671–1681. [\[CrossRef\]](#)
- Losi, A.; Russo, M. Dispersed Generation Modeling for Object-Oriented Distribution Load Flow. *IEEE Trans. Power Deliv.* **2005**, *20*, 1532–1540. [\[CrossRef\]](#)
- Chen, H.; Chen, J.; Shi, D.; Duan, X. Power flow study and voltage stability analysis for distribution systems with distributed generation. In Proceedings of the IEEE Power Engineering Society General Meeting, Montreal, QC, Canada, 18–22 June 2006; pp. 1–8. [\[CrossRef\]](#)

29. Naka, S.; Genji, T.; Fukuyama, Y. Practical equipment models for fast distribution power flow considering interconnection of distributed generators. In Proceedings of the Power Engineering Society Summer Meeting Conference Proceedings, Vancouver, BC, Canada, 15–19 July 2001; pp. 1007–1012. [[CrossRef](#)]
30. Nehrir, H.; Wang, C.; Shaw, S. Fuel cells: Promising devices for distributed generation. *IEEE Power Energy Mag.* **2006**, *4*, 47–53. [[CrossRef](#)]
31. Shahnia, F.; Majumder, R.; Ghosh, A.; Ledwich, G.; Zare, F. Voltage imbalance analysis in residential low voltage distribution networks with rooftop PVs. *Electr. Power Syst. Res.* **2011**, *81*, 1805–1814. [[CrossRef](#)]
32. Singh, A.K.; Singh, G.K.; Mitra, R. Some Observations on Definitions of Voltage Unbalance. In Proceedings of the 39th North American Power Symposium (NAPS), Las Cruces, NM, USA, 30 September–2 October 2007; pp. 473–479. [[CrossRef](#)]
33. Das, D.; Nagi, H.; Kothari, D. Novel method for solving radial distribution networks. *IEE Proc.-Gener. Transm. Distrib.* **1994**, *141*, 291–298. [[CrossRef](#)]
34. Radial Distribution Test Feeders. Available online: <http://sites.ieee.org/pes-testfeeders/resources> (accessed on 2 August 2021).